Monte Carlo Simulation Study of the Induced Deformation of Polymer Chains Dissolved in Stretched Networks

Andrew J. Haslam[†]

Department of Chemistry, University of Sheffield, Sheffield S3 7HF, U.K.

George Jackson*

Department of Chemical Engineering and Chemical Technology, Imperial College of Science, Technology and Medicine, Prince Consort Road, London SW7 2BY, U.K.

Tom C. B. McLeish

I.R.C. in Polymer Science and Technology and Department of Physics and Astronomy, University of Leeds, Leeds LS2 9JT, U.K.

Received February 10, 1998; Revised Manuscript Received June 8, 1999

ABSTRACT: We examine the preferential alignment of flexible hard-sphere polymer chains along a direction defined by a network of parallel hard rods. For relatively short chains (of 50 hard-sphere segments) we are able to quantify the alignment using a function, ϕ, which we have called the "nonsphericity" and which is analogous to the nematic order parameter P_2. Using this function, we show the alignment to be a weakly increasing function of the density of the chains and a much more strongly decreasing function of the separation of the rods comprising the network. In particular, for shorter chains, we demonstrate the presence of alignment even in the dilute regime, which is unexpected. Using three-dimensional distribution and scattering functions, we demonstrate preferential alignment for longer chains (of 2000 hard-sphere segments) at a density corresponding to the crossover between the dilute and semidilute regimes, although we see no evidence of alignment in the dilute region in this case.

1. Introduction

Deuterium nuclear magnetic resonance (DMR) has been used extensively to study the orientational order induced in stretched rubber networks.[1−9] Spectra obtained feature a characteristic doublet structure, both for network chains and for free chains diffusing in the network. It has been shown[9] that the classical description of a network cannot explain the existence of such a doublet structure, which suggests the presence of orientational interactions between segments; in the classical picture there are no such orientational interactions, and any distortion would be due only to entanglements of the free chains with cross-links in the network.

Scattering experiments have also provided evidence which may be interpreted as suggesting induced alignment. Displayed as contour plots in orthogonal directions, scattering functions appear as concentric circles for isotropic systems. Alignment in one direction gives rise to elongation of the scattering pattern along the perpendicular axis, so that the plot may, for example, take on an elliptical appearance. In a formal theoretical treatment of a polymeric solvent in a network, Edwards and McLeish[10] have produced scattering functions with a distinctive "lozenge" type appearance when displayed as contour plots, which they have likened to those seen experimentally by Bastide et al.[11] Shortcomings in the classical explanation are demonstrated by the experiments of Straube et al.[12] who see "lozenge" shaped scattering patterns in equilibrium experiments where dissolved chains have relaxed. Read and McLeish[13] have accounted quantitatively for "lozenge" scattering experiments on networks by identifying a more mobile chain fraction arising from dangling ends. Other experimental studies have given rise to scattering patterns known generally as "butterfly" or "bow tie" patterns (e.g., refs 11, 14, and 15), which are recognized as typical for nematic polymers[16,17] and which have been produced in recent Monte Carlo simulations of these.[18]

Read and McLeish[13] identify butterfly patterns as arising from a combination of elastic inhomogeneities and translationally mobile sections. We mention in passing the companion study of Boué et al.[19] to the DMR study of Deloche et al.[3] Using small angle neutron scattering (SANS) to study the same system as that examined by Deloche et al. (the samples were from the same source), Boué et al. found no evidence of induced alignment in free chains sorbed in the network, whereas the DMR study had indicated such alignment. To account for the apparent contradiction, these workers proposed that alignment might be present at short length scales (detectable by DMR), while at the longer length scales examined in the scattering experiments, it was lost. In their picture, the presence of hairpin bends in the chains could account for this.

Induced alignment has been demonstrated in other simulation studies, for example, the lattice Monte Carlo work of Deloche and co-workers[20,21] and the molecular dynamics work of Baljon et al.[22] on a bead−spring polymer network model.

In this paper, we use Monte Carlo simulation techniques to examine the effect of a constraining network on systems of flexible, tangent, hard-sphere chains, which we have already characterized for nonconstrained systems.[23]

[†] Current address: Materials Science Division, Argonne National Laboratory, Argonne, IL 60439.

10.1021/ma9802125 CCC: $18.00 © 1999 American Chemical Society
Published on Web 10/05/1999

2. Simulation Technique

Our model of hard-sphere polymer chains and the simulation details have been described in earlier work on the crossover scaling of an unconstrained system;[23] polymer molecules, represented by flexible chains of tangent hard-sphere segments, are placed in a cubic simulation cell, and Monte Carlo simulations using a reptation algorithm are used to establish the equilibrium properties of the system in the canonical (NVT) ensemble. We now represent the network, in a very crude fashion, as a square array of parallel hard cylinders of diameter equal to that of the hard-sphere segments; on the xy plane of the simulation box, a square array of circles is laid out, which become infinitely long cylinders when projected a distance equal to the box length, l, in the orthogonal (z) direction, due to the effect of the periodic boundary conditions. The free chains are treated exactly as in ref 23, but now the chains are excluded by the cylinder network as well as the self-exclusion of the polymer backbone. The intention is to establish whether there will be any alignment in the flexible chains induced by that of the array, by means other than an explicit local nematic coupling, so it is unnecessary to complicate the issue with cross-links. In any case, cross-links could not be placed further than a box length apart due to constraints of periodicity, and for high-density systems, it would no longer be possible to retain a model in which the dissolved chains were short compared to the cross-link distance. For this reason, our rudimentary representation, although unrealistic, is perhaps better equipped to answer our simple question.

To ensure the ergodicity of a simulation, the central segment of a chain may be labeled and followed to see how many reptation moves are required, on average, until the central segment becomes a chain end, when the label is passed to the segment then forming the center of the chain. Typical simulation runs for low-density systems were equilibrated for $\sim 6 \times 10^7$ moves, with averaging carried out over a further $\sim 6 \times 10^8$ moves; end-center exchanges for 2000 -segment chains take place on average after $\sim 10^6$ reptation moves for such systems, and the Monte Carlo acceptance rate is ~67%. Systems of high density were equilibrated over a few hundreds of millions of moves as necessary and averaged over a few thousands of millions; for the highest density simulations described in this paper, the frequency of end-center exchanges is slightly reduced to approximately one every 3−4 million moves and the Monte Carlo acceptance rate to ~65%.

To characterize the system, we have calculated functions as follows: the end-to-end distance $R(N)$; the spacial separation of pairs of segments as a function of their connective separation, $r(n)$; the pair radial distribution function $g(r)$, defined simply as the number density of monomer segments at a distance r from a given monomer, averaged over all monomers; the Fourier transformation of the radial distribution to give the scattering function, $s(k)$:

$$s(k) - 1 = 4\pi\rho \int_{-\infty}^{\infty} r^2 g_f(r) \frac{\sin(kr)}{kr}\, dr \qquad (1)$$

Here, $g_f(r)$ is the normalized, fluid-type function. Our calculation of these functions has been described in more detail in ref 23. In addition to these, we now introduce two further functions designed to detect any induced anisotropy. The first of these is a simple function, which we call the nonsphericity, denoted by ϕ.

2.1. Nonsphericity, ϕ. It is natural to imagine chains, in an isotropic environment, coiling up to form a roughly spherical shape. In fact, however, they do not, as Kuhn[24] pointed out as long ago as 1934; the degree of asphericity of chains was the subject of several studies in the 1970s[25−29] which showed that the coils are quite strongly aspherical; e.g., Šolc and Stockmayer[25] sum up, "... it must be concluded that the random flight chain usually looks far more like a cake of soap than a tennis ball." With hindsight, it is "obvious" that the coils will be aspherical purely on entropic grounds (there will be many more ways for the coil to be nonspherical). Fortunately for us, however, over time the coil must be spherically symmetrical on average, for there is no preferred direction for any distortion.

If we now consider our simulations of chains constrained by an array of cylinders, the natural intuition would suggest that any distortion would be manifest in the averaged shape becoming ellipsoidal. In the earlier studies, instantaneous asphericity was measured by considering, e.g., the three principal components, $L_1 \leq L_2 \leq L_3$, of the radius of gyration evaluated along the three principal axes of inertia.[25] We need consider nothing so complicated for our averaged asphericity, however, for in our model, we know in advance that the principal axis will lie along the direction of the network rods. We calculate a simple function which we denote by ϕ:

$$\phi = \frac{1}{2}\left\{\frac{2\langle R_z^2\rangle - \langle R_x^2\rangle - \langle R_y^2\rangle}{\langle R^2\rangle}\right\} \qquad (2)$$

where $\langle R^2\rangle$ represents the mean-square end-to-end distance of the chain, $\langle R_z^2\rangle$ is the average of the square of the z component of the end-to-end vector, $\mathbf{R}$, and similarly for x and y. Thus, for a perfectly nonaligned, or isotropic, system in which $\langle R_z^2\rangle = \langle R_x^2\rangle = \langle R_y^2\rangle$, the nonsphericity $\phi = 0$, whereas for perfect alignment along the z direction (i.e., with each bond angle fixed at 180° and the chain is effectively a rigid rod of spheres), $\phi = 1$.

It can be seen that this function is in some way analogous to the nematic order parameter P_2, or S, used to describe orientational ordering in liquid crystals, where $P_2 = {}^1/_2(3\langle\cos^2\theta\rangle - 1)$, and the angle θ corresponds to that between the molecular axis and a director:

$$-\langle R_x^2\rangle - \langle R_y^2\rangle = \langle R_z^2\rangle - \langle R^2\rangle \qquad (3)$$

Therefore

$$\phi = \frac{1}{2}\left\{\frac{3\langle R_z^2\rangle - \langle R^2\rangle}{\langle R^2\rangle}\right\} = \frac{1}{2}\left\{3\frac{\langle R_z^2\rangle}{\langle R^2\rangle} - 1\right\} \qquad (4)$$

Now, $R_z/R = \cos\theta$ for some θ, so $\langle R_z^2/R^2\rangle \equiv \langle\cos^2\theta\rangle$. In fact, since R_z and R are not independent, we cannot write $\langle R_z^2\rangle/\langle R^2\rangle = \langle\cos^2\theta\rangle$, so ϕ is not equivalent to P_2, but clearly there is some analogy between these two quantities.

2.2. Vector-Dependent Correlation Function and Structure Factor. Our second principal method for detecting anisotropy is the calculation and examination of vector distribution and scattering functions. In the previous publication,[23] we have described the calculation of segment−segment radial distribution functions, both for segments of the same chain, $g_s(r)$, and for those of the whole system, $g(r)$; we have also described the Fourier transformation of these to provide the structure factor, or scattering function, $s(k)$. For the network system, in addition to these distribution functions we calculate $g(\mathbf{r})$. This vector distribution function, which can be described as the number density at position $\mathbf{r}$ relative to the origin monomer, can show up distortion in the overall shapes of the chains, since it is not subject to the radial averaging of $g(r)$.

In this case one imagines, instead of the origin monomer being surrounded by spherical shells of width δr, as would be the case for the radial $g(r)$, that it is surrounded by cubic boxes extending in each of the Cartesian directions to the edge of the box. In principle, therefore, one can include all the monomers in the simulation in this accumulation, contrasting the radial equivalent in which one cannot include segments at greater distances than half the box length without including some monomers twice via the overlap of the spherical shell into the periodic images.

One cannot display this function, since to do so would require a four-dimensional picture: one dimension each for the Cartesian axes x, y, and z, and one for g. However, on average, our system possesses cylindrical symmetry and thus we are able to make the transformation to a function which may be displayed using three dimensions. We define $r^{*2} = x^2 + y^2$ to produce the function $g(r^*,z)$. Thus, the cubic bins which made up the full vector function are now grouped together into bins the shape of metal washers.

When the transformation $r^{*2} = x^2 + y^2$ is made, and we switch instead to the washer-shaped bins, it is important to note that even though we are accumulating the histogram from real space, the simulation itself is periodic. If the length of the simulation box is l, then there must be zeroes in the full distribution function at $g(l,0,0)$, $g(0,l,0)$ and $g(0,0,l)$ as a result of the periodicity. This is no problem at low densities, when the chain length is short compared to l, but at higher densities, when they are of the same order of magnitude, these zeroes are artifacts of the method and must not be confused with real effects. We call this the periodic anomaly in the distribution function.

The structure factor is related to the pair distribution function by the Fourier transform[30]

$$s(\mathbf{k}) = 1 + \rho \int_{-\infty}^{\infty} \mathrm{e}^{-i(\mathbf{k},\mathbf{r})}\, g_f(\mathbf{r})\, \mathrm{d}\mathbf{r} \qquad (5)$$

i.e., putting $\mathbf{r} = (x, y, z)$

$$s(k_x,k_y,k_z) = 1 + \rho \int\int\int \mathrm{e}^{-i(k_x x + k_y y + k_z z)}\, g_f(x,y,z)\, \mathrm{d}x\, \mathrm{d}y\, \mathrm{d}z \qquad (6)$$

where $\rho = N/V$ is the system number density, as usual, and $g_f(\mathbf{r})$ represents the conventional fluid radial distribution function ($g(\mathbf{r}) = \rho g_f(\mathbf{r})$).

The derivation of the equivalent formula to transform $g(r^*,z)$ is given in an appendix. The result is as follows:

$$s(k_{r^*},k_z) = 1 + 2\rho\pi \int_{-\infty}^{+\infty} \cos(k_z z)\, \mathrm{d}z \int_0^{+\infty} r^* g(r^*,z)\, J_0(r^* k_{r^*})\, \mathrm{d}r^* \qquad (7)$$

Random numbers for the simulations were generated using the routine *ran2* from ref 31. Simulations were carried out on Silicon Graphics R4000 Indigo, R4400 and R5000 Indy, and DEC α workstations.

3. Results

3.1. Effect of Cylinder Separation and Density on ϕ for Short Chains. The separation of the cylinders may be controlled either by increasing the number density of cylinders or by retaining the same lattice and varying the diameter of the cylinders, which is also that of the sphere segments. Density was varied simply by including more chains in the simulation, while fixing the segment diameter; simulations were then carried out in the usual way. Clearly, in this scenario, it is necessary to choose a suitable length for the chains that is long enough for each to be recognizably polymeric in its behavior yet which allows maximum scope for variation in the system density. Thus, it was necessary to judge what constituted the shortest possible chain that was still recognizably polymeric in its behavior. From inspection of the linearity of $R(N)$ and $r(n)$ plots produced in our study of the unconstrained polymer,[23] we judged chains of 50 segments to be most appropriate. It would clearly be desirable to try to span the crossover region from swollen to semidilute. In the simulations without the cylinder network[23] we have characterized this crossover for the isotropic system; in the direction of increasing density, the crossover begins at a packing fraction $\eta \sim 0.001$ and ends at $\eta \sim 0.15$. The packing fraction, a measure of reduced density, is defined as follows:

$$\eta = \frac{\pi}{6}\sigma^3 \frac{N_{\mathrm{seg}}}{V} \qquad (8)$$

N_{seg} represents the number of sphere segments present, σ the diameter of these segments, and V the volume accessible to the chains (in this case, the system volume; however, in the network simulations, V represents the system volume less that of the rods). Unfortunately, due to computational restrictions, it was not feasible to span this range. For example, an isolated chain in a square lattice of $49 = 7 \times 7$ cylinders requires a segment diameter of about $\sigma = 0.033l$ to satisfy a packing fraction of $\eta = 0.001$. Retaining this value of the diameter and increasing the number of chains to the maximum which could be simulated in a reasonable time on our machines, i.e., 40, correspond to a packing fraction of only $\eta = 0.04$. In general, we found that we could not span the crossover region entirely with any given set of parameters.

The values of the nonsphericity parameter, ϕ, obtained in simulations at various values of packing fraction and cylinder spacing are set out in tabular form (see Tables 1−4). Simulations carried out on chains of 50 segments, in an environment without cylinders, gave values of $\phi = 0$ to two decimal places. Consequently we can conclude that, for the cylinder system where $\phi > 0$, there is alignment even at low density. If we look within the tables we see that there is, perhaps surprisingly,

Table 1. Nonsphericities of 50-Segment Chains in a 10 × 10 Cylinder Array

segment diameter, σ/l	number of chains	chain packing fraction, η	nonsphericity, ϕ	cylinder separation/σ
0.015	1	0.00009	0.042	6.7
0.015	2	0.00018	0.043	6.7
0.015	5	0.00045	0.043	6.7
0.015	10	0.0009	0.042	6.7
0.015	20	0.0018	0.043	6.7
0.015	40	0.0036	0.043	6.7
0.015	80	0.0072	0.043	6.7
0.03	1	0.00076	0.119	3.3
0.03	2	0.0015	0.119	3.3
0.03	5	0.0038	0.119	3.3
0.03	10	0.0076	0.119	3.3
0.03	20	0.015	0.120	3.3
0.03	40	0.03	0.122	3.3
0.03	80	0.061	0.125	3.3
0.043	1	0.0024	0.266	2.3
0.043	2	0.0049	0.267	2.3
0.043	5	0.012	0.272	2.3
0.043	10	0.024	0.276	2.3
0.043	20	0.049	0.293	2.3
0.043	40	0.097	0.323	2.3

Table 2. Nonsphericities of 50-Segment Chains in a 7 × 7 Cylinder Array

segment diameter, σ/l	number of chains	chain packing fraction, η	nonsphericity, ϕ	cylinder separation/σ
0.043	1	0.0022	0.119	3
0.043	2	0.0045	0.119	3
0.043	5	0.011	0.119	3
0.043	10	0.022	0.123	3
0.043	15	0.034	0.124	3
0.043	20	0.045	0.127	3
0.043	25	0.045	0.128	3
0.043	30	0.056	0.126	3
0.043	35	0.067	0.126	3
0.043	36	0.081	0.125	3
0.043	38	0.085	0.126	3
0.043	40	0.090	0.121	3

little relationship between ϕ and the packing fraction or density. It is worth examining this in a little more detail.

First, we consider the set of simulations from Table 1, describing chains of segments with diameter $\sigma = 0.015l$, and we observe that the (nonzero) value of ϕ is more or less invariant despite an 80-fold increase in the packing fraction. The most obvious explanation might be that the separation of the cylinders is large compared with the size of the chains. This, however, is demonstrably not the case if we examine the average end-to-end distances of the chains from the same simulations, which are shown in Table 3. Returning to Table 1, we can see that with each increase in segment diameter, and the corresponding decrease in cylinder separation, there is a marked increase in the value of ϕ. This is entirely what one would expect if chain−cylinder interactions dominate anisotropy (rather than chain−chain interactions).

Finally, by comparing the data in Table 2 with the second set of data in Table 1 relating to chains of segments with diameter $\sigma = 0.03l$, we can see that the values of ϕ in these two instances are very similar. Since in these two sets of simulations we have altered both the segment diameter and the number of cylinders in the array, the only remaining parameter which is similar is the cylinder separation. We are drawn therefore to the idea that the principle factor influencing

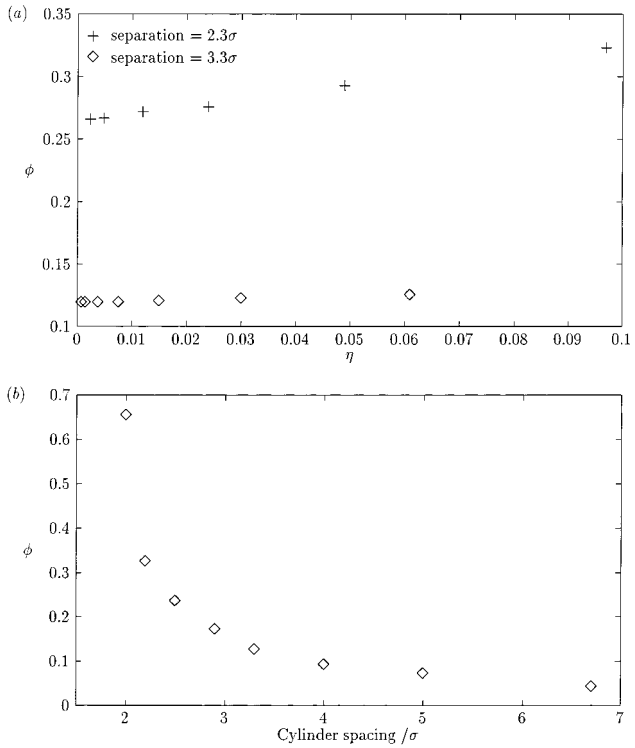

Figure 1. (a) Effect of chain packing fraction on ϕ for 50-segment chains. (b) Effect of cylinder spacing on ϕ for 10 × 50-segment chains.

Table 3. Sizes of 50-Segment Chains with $\sigma = 0.015l$ in a 10 × 10 Cylinder Array

number of chains	chain packing fraction, η	$\langle R \rangle$	cylinder separation/σ
1	0.00009	11.848 ± 0.022	6.7
2	0.00018	11.853 ± 0.023	6.7
5	0.00045	11.841 ± 0.022	6.7
10	0.0009	11.835 ± 0.021	6.7
20	0.0018	11.821 ± 0.026	6.7
40	0.0036	11.423 ± 0.068	6.7
80	0.0072	11.729 ± 0.024	6.7

Table 4. Effect of Cylinder Distribution on Nonsphericity for 10 × 50-Segment Chains with Segment Diameter $\sigma = 0.05l$

number of cylinders in array	approximate cylinder separation/σ	nonsphericity, ϕ	chain packing fraction, η
9	6.7	0.042	0.033
16	5	0.071	0.034
25	4	0.091	0.034
36	3.3	0.125	0.035
49	2.9	0.171	0.036
64	2.5	0.235	0.037
81	2.2	0.325	0.039
100	2	0.654	0.041

anisotropy is the separation of the cylinders (scaled in terms of the segment diameter).

The data given in Table 4 further illustrate the pronounced influence of cylinder separation. These data are displayed graphically, alongside that from Table 1, in parts a and b of Figure 1, which clearly demonstrate the relative magnitudes of the effects of chain density and of cylinder spacing on ϕ. In Figure 1a, we see the increase in ϕ associated with an increase of chain packing fraction from $\sim 10^{-4}$ to $\sim 10^{-1}$. Although the trend is plainly upward, the nature of the dependence is not so clear: a linear relationship looks to be the best

guess; the magnitude of the increase across this span is about 0.06. In Figure 1b, showing the effect of cylinder spacing, there is an associated increase in the packing fraction of 0.033−0.041. The magnitude of variation in ϕ, however, is almost 0.7, or roughly 10 times the spread seen in Figure 1a. This clearly demonstrates a far greater dependence on the cylinder separation than that on the density of confined chains. Although the curve looks quite smooth, it is not well approximated by any simple function, so a mathematical description of the dependence is not easy to find.

3.2. Anisotropy of Long Chains via Distribution Functions and Structure Factors. To complement the analysis using nonsphericities, in which shorter chains were used to enable the greatest possible control of density, we chose to simulate single chains of much greater length, i.e., 2000 hard-sphere segments. To enable us to better relate our results to experimental work, in this case we employ a different method to detect the anisotropy in our systems: the calculation of vector dependent distribution functions and their Fourier transformation into structure factors, or scattering functions. These are functions that can be plotted in three dimensions and thus offer visual evidence of any distortion.

Accumulating pair distribution functions in three dimensions is an expensive process both in CPU time and also, in particular, in the storage required. Taking as few as 100 bins in each of the Cartesian directions necessitates a triple loop with of the order of 100 × 100 × 100 operations for each accumulation and similarly creates a million bins, or storage locations, in all. This analysis was therefore restricted to four carefully chosen systems. Clearly, the nonnetwork system, containing no cylinders, is required as the reference system. Ideally, the other three classes of system would be the dilute or swollen regime, the melt or Gaussian regime, and one point in the semidilute region, all including the constraint of a rod network. Unfortunately, it was not possible in practice to examine the melt. The usual problems associated with simulation at high density, of difficulty in generating a starting configuration, and of difficulty in sampling phase space within sensible time scales, were compounded by the presence of the rods; we found that configurational bias techniques provided no solution for chains of this length. We know from our preliminary study,[23] in which the errors in the simulations were examined in detail, that the error associated with simulations of melt chains on a practical time scale is much greater than that for the systems we have chosen. It is desirable in this comparative study that the errors in all the simulations are of the same order of magnitude, whereas this would not be true for the melt system, and thus it was not included in the study. For comparison, a system of Gaussian chains in an excluding network was also simulated; in this calculation, there was no interaction between segments of the chain, but there was a hard repulsion (excluded volume interaction) between the chain segments and the cylinders. Plots of these functions are displayed, in the reduced cylindrical form with $r^* = \sqrt{(x^2 + y^2)}$ as described earlier. For these simulations, the rod network was chosen to be one of 100 cylinders in a 10 × 10 square array.

3.2.1. Constrained Swollen Chain. The next set of results pertains to simulations of a swollen 2000 segment chain, with the packing fraction set at $\eta = 10^{-7}$,

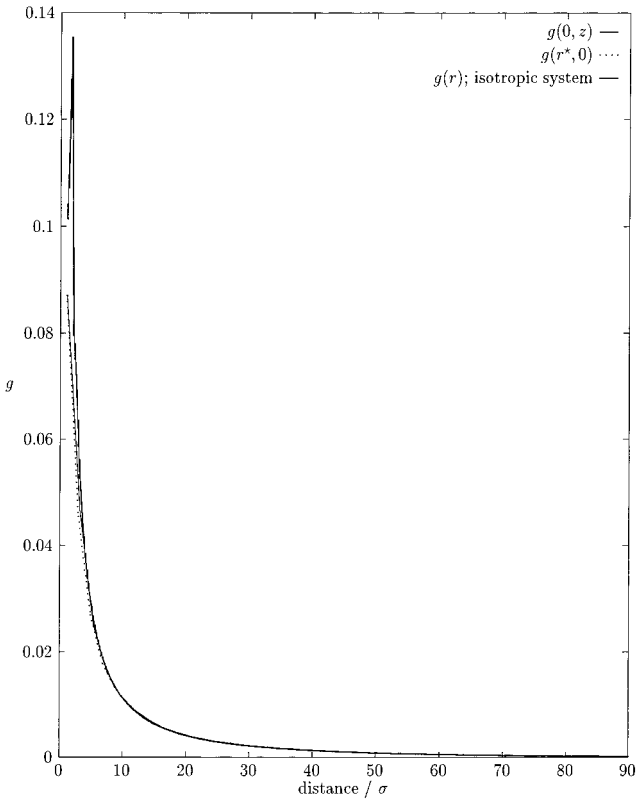

Figure 2. Distribution function $g(r)$ for isotropic system and slices through $g(r^*,z)$ for constrained swollen system ($\eta = 10^{-7}$ and 100 cylinder array).

in a network of 100 rods; for this system, the segment diameter is $\sigma = 4.57 \times 10^{-4}l$ and the cylinder spacing is 219σ. Figure 2 shows the superimposed slices through $g(r^*,z)$ together with the "radial" function calculated from simulation of the equivalent system with no cylinders. The agreement of these curves is excellent. It is difficult to distinguish the individual curves for most of the range, suggesting that there is no discernible anisotropy, as well as providing reassurance that the accumulation and re-binning of the vector function has been carried out correctly. There is no evidence of a periodic anomaly in this plot; its appearance at this density would have been alarming, since even the fully extended chain cannot interfere with its periodic image.

Figure 3 shows the scattering function calculated from the data relating to the constrained swollen chain, in the form of a contour plot; no anisotropy is obvious here either. Finally, for this system, Figure 4 shows slices taken through the surface of the scattering function, together with $s(k)$ for the equivalent system without the constraint of the network. The two slices for the constrained system agree precisely at very low k, through what could be described as the "polymer region"; the agreement confirms that there is no anisotropy. Although these curves do not quite agree with that for the nonconstrained system at the peak, there is a period of agreement of all three curves as k increases, before the slice through k_z begins to deviate. This latter function arises from data which has not benefited from the averaging that is a consequence of rebinning $g(x,y,z)$ into $g(r,z)$, which may explain this small divergence; in any case, the divergence is at high k and would represent short-range distortion. The accumulation of the radial $g(r)$ implicitly involves a further degree of averaging still (in the sense that the

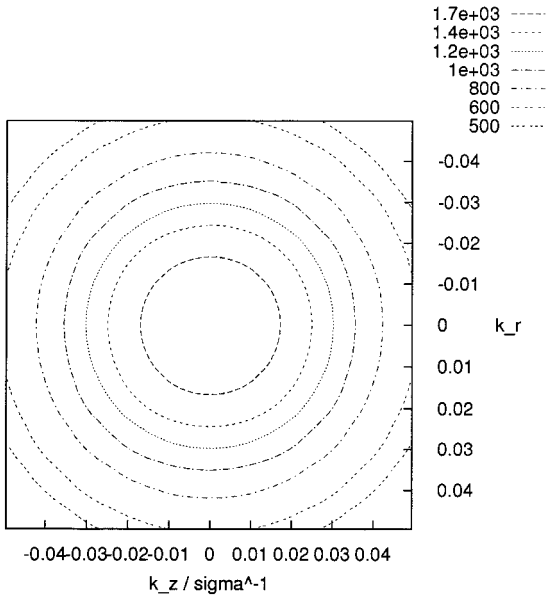

Figure 3. Scattering function $s(k_r^*,k_z)$ for constrained swollen system ($\eta = 10^{-7}$ and 100 cylinder array): contour plot. The value of the function decreases from the inner to the outer curves.

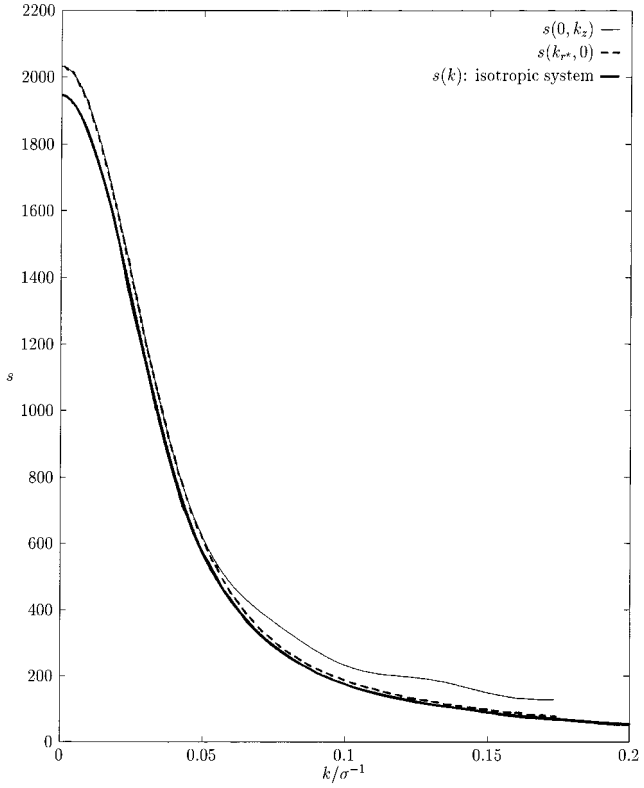

Figure 4. Comparison of scattering function $s(k)$ for isotropic system with slices through $s(k_r^*,k_z)$ for constrained swollen system ($\eta = 10^{-7}$ and 100 cylinder array).

histogram bins at a given distance are larger), so that both the function $s(k)$ and slice $s(k_{r^*},0)$ are functions of more highly averaged data.

The analyses above reveal no evidence of sympathetic alignment of chains along the cylinder axis at this low density.

3.2.2. Unconstrained and Constrained Semidilute Chains. In our earlier work,[23] we have characterized the semidilute region for the unconstrained system;

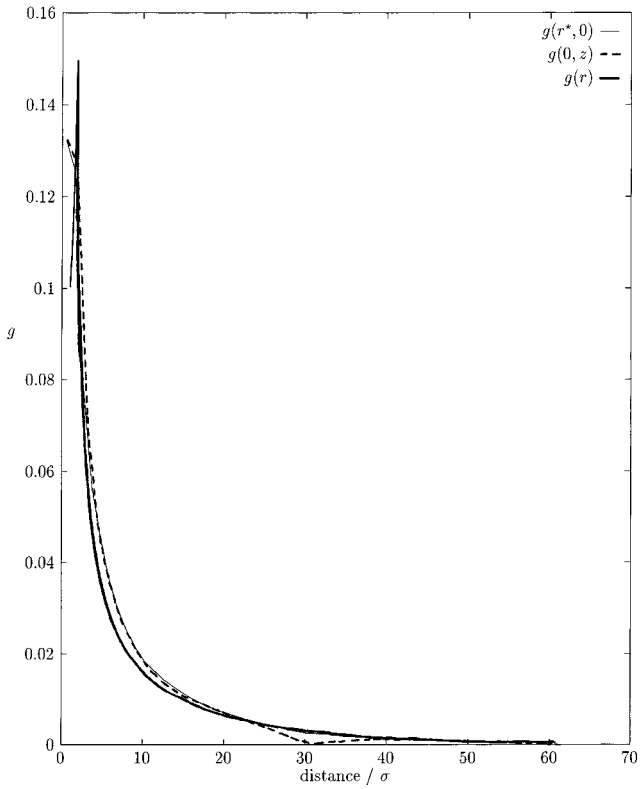

Figure 5. Distribution function $g(r)$ and slices through $g(r^*,z)$ for unconstrained semidilute system ($\eta = 0.025$).

from this we chose a packing fraction of $\eta = 0.025$, which lay well inside this region. Clearly one would expect that the unconstrained system should be isotropic. This can be confirmed by viewing perpendicular slices through the pair distribution function $g(r^*,z)$.In Figure 5, slices through $z = 0$ and $r = 0$ are superimposed, together with the radial $g(r)$. The two slices are almost indistinguishable, and agree well with the radial function. Indeed, it is reassuring to see that these curves coincide so closely, since this shows that the more complicated accumulation and transformation of the cylindrical function has been accomplished correctly. The coincidence of the two slices show that the decay in r and z are equivalent; there is no sign of anisotropy. It is interesting to see the periodic anomaly appearing clearly in the slice $g(0,z)$, whereas it is only just apparent in the slice $g(r^*,0)$, and completely absent in the radial $g(r)$; each appeal to symmetry in some sense averages out this effect.

The same data is Fourier transformed to the scattering function; the contours of this are displayed in Figure 6. The plot shows that there is no anisotropy in the system; elongation in the z, direction would be manifest as elongation in the perpendicular direction in reciprocal space, so that this contour plot would appear stretched in the k_r^* direction, and vice versa. Once again, superimposition of perpendicular slices from the surface confirm the absence of anisotropy, although in the interests of brevity this plot is not included.

The next set of figures depicts simulations of a system equivalent to that we have just been describing, except that a network of 100 hard cylinders in a square lattice has been introduced. In this case the segment diameter is $\sigma = 2.82 \times 10^{-2} l$ and the cylinder spacing is 3.55σ. Figure 7 shows the superimposed slices through $g(r,z)$ together with the "radial" function. On this occasion,

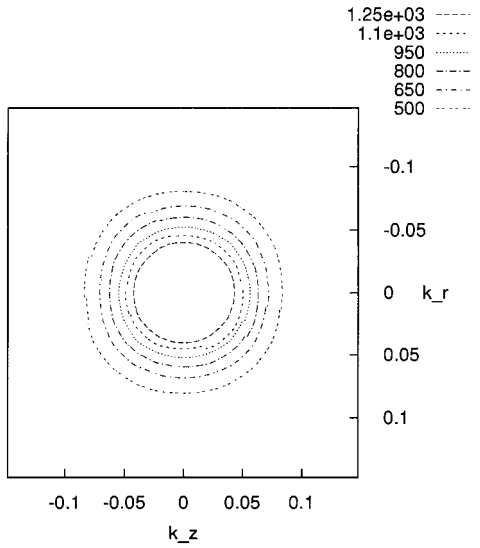

Figure 6. Scattering function $s(k_r^*,k_z)$ for unconstrained semidilute system ($\eta = 0.025$): contour plot. The value of the function decreases from the inner to the outer curves.

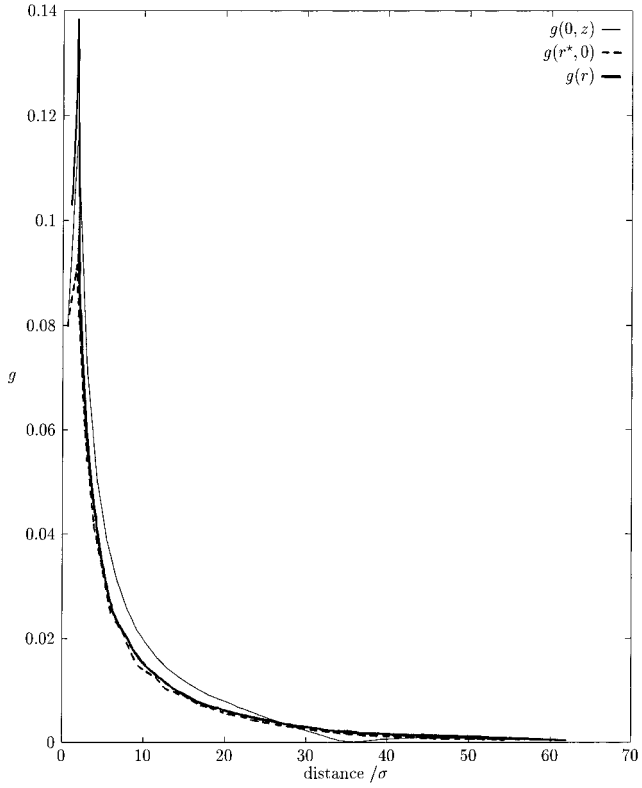

Figure 7. Distribution function $g(r)$ and slices through $g(r^*,z)$ for constrained semidilute system ($\eta = 0.025$ and 100 cylinder array).

the curves do not coincide; this can just be made out on the complete function, but can be seen more clearly in Figure 8, where the tail region of the graph is highlighted and shown together with the same region for the earlier data for the radially symmetric system. Except in the region of the periodic anomaly, the value of $g(0,z)$ is always greater than that of $g(r^*,0)$, with $g(r)$, the radially averaged function, lying comfortingly between the two. For the first time we see clear evidence of anisotropy. Once again the periodic anomaly is clearly evident in the slice through $r^* = 0$, however it appears at a slightly higher value of z. Retaining the same value of packing fraction after introducing the cylinders

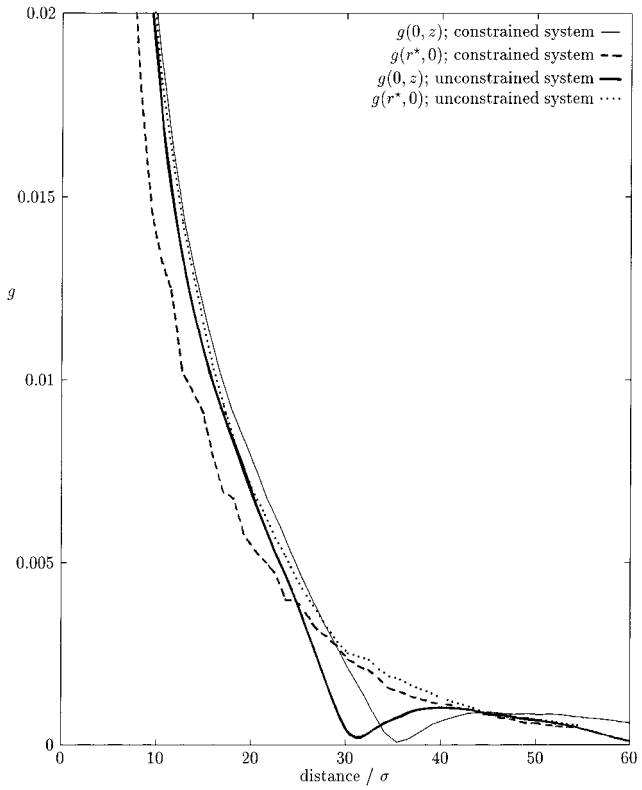

Figure 8. Comparison of slices through the distribution function $g(r^*,z)$ for isotropic and constrained semidilute systems ($\eta = 0.025$ and 100 cylinder array).

requires a slightly smaller segment diameter (as has been mentioned earlier), which is equivalent to a slightly larger simulation box length (to $\sim 35\sigma$ from $\sim 34\sigma$). Thus, we would expect a small translation of the local minimum in this curve; that the translation is larger than σ is probably due to the alteration in histogram-bin size resulting from the change in the simulation box. Neither minimum quite touches the axis, but that in the g of the constrained system is noticeably lower, suggesting that in the latter case the bin sizes may indeed be more appropriate.

The scattering function for this system is shown in the contour plot of Figure 9. One can again detect the anisotropy, with the contours elongated in the k_r^* direction relative to k_z, indicating that the chain is deformed with an elongation along the direction of the cylinders. The contour plot reveals the same type of anisotropy as seen in the melt "lozenge" experiments and theoretical predictions, but to a much weaker extent. It takes on a component with P_4 symmetry at intermediate k; there is a slight flattening of the contours along the diagonals of the plots, which is the beginning of the "lozenge" type pattern. From our earlier work[23] we believe that the screening length ξ for the unconstrained system at this density lies at approximately 100σ; this would correspond to a wave vector of $k \approx 0.01\sigma^{-1}$ which, although a little lower, is of the order of magnitude over which the distortion in Figure 9 is seen.

Kamien and Grest[18] have simulated nematic polymer molecules using a "pearl necklace" of hard spheres; stiffness was provided by a bending energy parameter. These workers succeeded in producing a bow tie scattering pattern, but at a packing fraction of $\eta = 0.25$—a much higher density than the semidilute system we have been describing. From their simulation at a

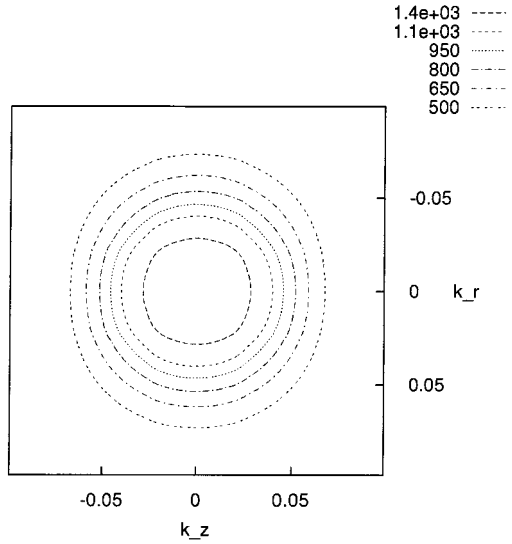

Figure 9. Scattering function $s(k_r^*, k_z)$ for constrained semidilute system ($\eta = 0.025$ and 100 cylinder array): contour plot. The value of the function decreases from the inner to the outer curves.

packing fraction of $\eta = 0.13$, still much higher than our semidilute value of $\eta = 0.025$, the scattering pattern is elliptical in appearance and qualitatively similar to that of Figure 9; we do not expect to produce a plot of "bow tie" appearance at the lower densities we have studied.

3.2.3. Constrained Gaussian Chain. A Gaussian chain, constrained by a network of cylinders, is also examined. The simulation is carried out as normal, except that the (repulsive) interaction between the chain segments is switched off, leaving only that between chain segment and cylinder. To define the separation of the cylinders, the packing fraction of the chains was again set at $\eta = 0.025$, matching as closely as possible earlier simulations; the corresponding cylinder spacing is again 3.55σ.

Again beginning with the perpendicular slices through the cylindrical distribution function, we can see in Figure 10 that the slice $g(0,z)$ lies clearly above $g(r^*,0)$, illustrating a distortion in the chain. $g(r)$ for an unconstrained Gaussian system is also displayed in this figure; at low values of r corresponding to only 2σ or 3σ, this function agrees closely with the slice $g(0,z)$, however as r approaches 5σ, $g(r)$ begins to decay a little more quickly, falling between the two slices until at the tail of the distributions all three merge quite closely. Closer examination of the tail shows the radial function and the slice $g(0,z)$ crossing over.

As would be expected for a chain with no self-interactions, the distribution functions all decay much more quickly than we are accustomed to seeing for self-excluding chains; in the latter case we do not expect to see the functions decay completely until about 60 to 80σ, whereas the functions representing the Gaussian chains approach zero after about 25σ. The values of g at and near the peak of the distribution functions are at least an order of magnitude larger than we see for self-excluding chains. Again, this is no surprise; when any number of segments may occupy the same space, the number density of segments close to the origin segment inevitably will be much higher.

The scattering function for this system is shown in Figure 11, where the anisotropy is again obvious. There is clear evidence of a relative elongation of the chain

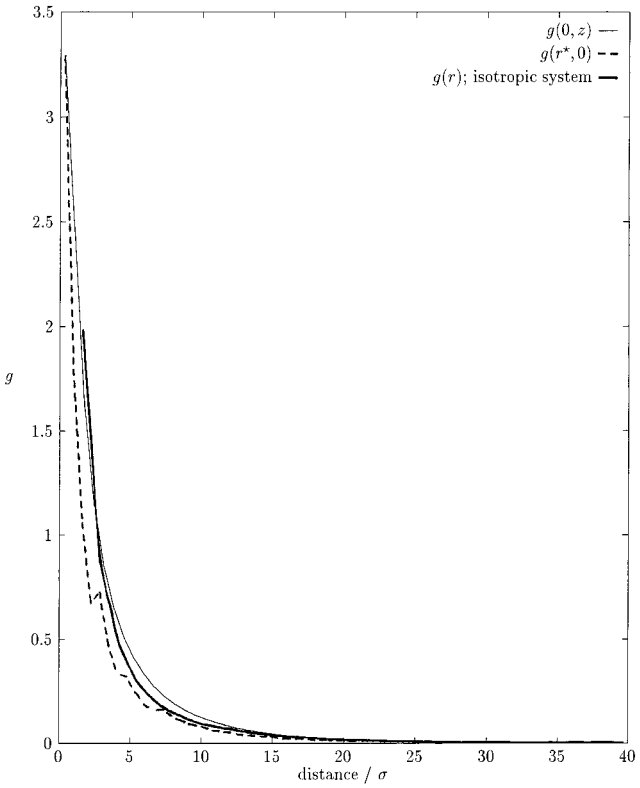

Figure 10. Distribution function $g(r)$ for isotropic system and slices through $g(r^*,z)$ for constrained Gaussian system ($\eta = 0.025$ and 100 cylinder array).

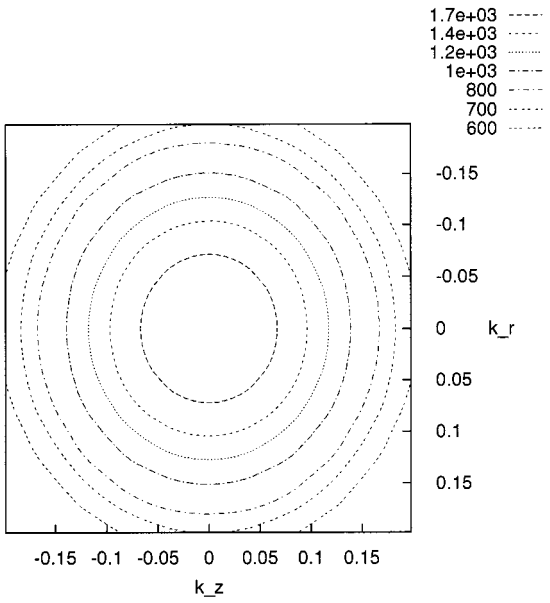

Figure 11. Scattering function $s(k_r^*,k_z)$ for constrained Gaussian system ($\eta = 0.025$ and 100 cylinder array): contour plot. The value of the function decreases from the inner to the outer curves.

along the cylinder, or z axis given by the elongation of the contours in the k_r^* direction. In this case, though, it is debatable whether there is any evidence of the characteristic "lozenge" appearance; there is a hint of some flattening of the contours along the diagonals of the patterns, but it is very subtle.

4. Concluding Remarks

In this study we have examined the preferential alignment of hard-sphere chain molecules along a

direction defined by a network of parallel hard rods. By simulating systems with varying numbers of 50-segment chains, at varying densities, we have clearly demonstrated such preferential alignment. For such systems, we have been able to quantify the degree of alignment using a function which we have called the nonsphericity, ϕ. Using this measure, we have shown the alignment to be a weakly increasing function of the density of the chains, and a much more strongly decreasing function of the separation of the rods comprising the network. In particular, we have been able to demonstrate alignment even in the dilute region, which is unexpected.

We have examined longer (2000-segment) chains using distribution and scattering functions. Using this method, we have not seen clear evidence of preferential alignment for our chains in the excluded-volume (dilute) regime. However, such evidence has been provided for chains in the semidilute region. There is a clear contrast between distribution and scattering functions accumulated in simulations of semidilute systems with and without the constraint of a network. The nature of this contrast indicates a deformation of the chain in the presence of the cylinders, such that the chain has been moderately elongated in the direction of the cylinders, and moderately compressed in the perpendicular plane. The same conclusion may be drawn in the case of Gaussian chains simulated in the environment of excluding cylinders.

We have not reproduced distinct "lozenge" shaped contour plots of the scattering functions, seen experimentally by Barea et al.[14] and Straube et al.[12] and predicted by Edwards and McLeish[10] and Read and McLeish,[13] but we have seen slight distortions in our scattering patterns which are a weaker manifestation of the same effect. As expected, we have not seen the so-called "bow-tie" patterns.

The question of alignment in equilibrium systems of confined chains is thus clearly answered for a simple model system. In our case, the alignment is due to excluded volume interactions between segments of the chain and the rods comprising the network.

Acknowledgment. We are very grateful to Alejandro Gil-Villegas, Kostas Daoulas, and Demetri Photinos for useful discussions. A.J.H. would like to thank the Centre for Molecular Materials of Sheffield University for the award of a University Scholarship. We also acknowledge support from the Royal Society (574005.G501/1992), from the European Commission (CI1*-CT94-0132) and from the Computational (GR/H58810-C91) and ROPA (GR/K34740) Initiatives of the EPSRC for computer hardware on which the calculations were performed.

Appendix A. Transformation of $g(r^*,z)$

The formula to transform $g(r^*,z)$ can be obtained as follows. We choose to make the transformation to cylindrical polar co-ordinates, so we make the substitution $x = r^* \cos\theta$, $y = r^* \sin\theta$, so that

$$r^* = \sqrt{x^2 + y^2} \tag{9}$$

Then

$$s(k_x, k_y, k_z) = 1 + \rho \int\int\int e^{-i(k_x r^*(\cos\theta)+k_y r^*(\sin\theta)+k_z z)} g_f(x,y,z)\, r^*\, dr^*\, d\theta\, dz$$

$$= 1 + \rho \int e^{-i(k_z z)}\, dz \int\int e^{-i(k_x r^*(\cos\theta)+k_y r^*(\sin\theta))} g_f(x,y,z)\, r^*\, dr^*\, d\theta \tag{10}$$

With the symmetry argument $g_f(x,y,z) = g_f(\sqrt{x^2+y^2},z) = g(r^*,z)$, we have

$$s(k_x,k_y,k_z) = 1 + \rho \int_{-\infty}^{+\infty} e^{-i(k_z z)}\, dz \int_0^{+\infty} r^* g(r^*,z)\, dr^* \int_{\text{period}} e^{-i(k_x r^*(\cos\theta)+k_y r^*(\sin\theta))}\, d\theta \tag{11}$$

We make the parametrization $k_x r^* = A \sin b$, $k_y r^* = A \cos b$, i.e., $b = \tan^{-1}(k_x/k_y)$, so that

$$\int_{\text{period}} e^{-i(k_x r^*(\cos\theta)+k_y r^*(\sin\theta))}\, d\theta = \int_{\text{period}} e^{-i(A(\sin b)(\cos\theta)+A(\cos b)(\sin\theta))}\, d\theta = \int_{\text{period}} e^{-iA(\sin(\theta+b))}\, d\theta = \int_{\text{period}} \cos(A\sin(\theta+b))\, d\theta - i\int_{\text{period}} \sin(A\sin(\theta+b))\, d\theta \tag{12}$$

$\int_{\text{period}} \sin(A \sin(\theta + b))$ will vanish since it is an integral of an odd function over a whole period. Therefore

$$s(k_r^*,k_z) = 1 + \rho \int_{-\infty}^{+\infty} e^{-i(k_z z)}\, dz \int_0^{+\infty} r^* g(r^*,z)\, dr^* \int_{\text{period}} \cos(A\sin(\theta+b))\, d\theta \tag{13}$$

Now, $1/\pi \int_{\text{half period}} \cos(A \sin(\theta + b))\, d\theta$ is the Bessel function, $J_0(A)$,[32] so

$$s(k_r^*,k_z) = 1 + 2\rho\pi \int_{-\infty}^{+\infty} e^{-i(k_z z)}\, dz \int_0^{+\infty} r^* g(r^*,z) J_0(A)\, dr^* \tag{14}$$

If we return to the parametrization, we can characterize A: $A \sin(b) = k_x r^*$, $A \cos(b) = k_y r^*$, therefore

$$A^2(\sin^2(b) + \cos^2(b)) = r^{*2}(k_x^{\,2} + k_y^{\,2})$$

and

$$A = r^*\sqrt{k_x^{\,2} + k_y^{\,2}} = r^* k_r^* \tag{15}$$

where

$$k_r^* = \sqrt{k_x^{\,2} + k_y^{\,2}}$$

Then

$$s(k_r^*,k_z) = 1 + 2\rho\pi \int_{-\infty}^{+\infty} e^{-i(k_z z)}\, dz \int_0^{+\infty} r^* g(r^*,z)\, J_0(r^* k_r^*)\, dr^* \tag{16}$$

We can further reduce this by noting that

$$\int_{-\infty}^{+\infty} e^{-i(k_z z)}\,dz = \int_{-\infty}^{+\infty} \cos(k_z z)\,dz - i\int_{-\infty}^{+\infty} \sin(k_z z)\,dz \quad (17)$$

The latter term is the integral of an odd function, and so vanishes. Thus

$$s(k_r^*,k_z) = 1 + 2\rho\pi \int_{-\infty}^{+\infty} \cos(k_z z)\,dz \int_0^{+\infty} r^* g(r^*,z) J_0(r^* k_r^*)\,dr^* \quad (18)$$

This was calculated using simple numerical quadrature; the Bessel function was calculated numerically using a routine from ref 31.

References and Notes

(1) Deloche, B.; Samulski, E. T. *Macromolecules* **1981**, *14*, 575.
(2) Deloche, B.; Samulski, E. T.; Herz, J. *J. Phys. Lett.* **1982**, *43*, 1763.
(3) Deloche, B.; Dubault, A.; Herz, J.; Lapp, A. *Europhys. Lett.* **1986**, *1*, 629.
(4) Sotta, P.; Deloche, B.; Herz, J.; Lapp, A.; Durand, D.; Rabadeux, J. C. *Macromolecules* **1987**, *20*, 2769.
(5) Sotta, P.; Deloche, B.; Herz, J. *Polymer* **1988**, *29*, 1171.
(6) Gronski, W.; Stadler, M.; Jacobi, M. *Macromolecules* **1984**, *17*, 741.
(7) Jacobi, M.; Stadler, M.; Gronski, W. *Macromolecules* **1986**, *19*, 2887.
(8) Litvinov, V.; Spiess, H. W. *Makromol. Chem.* **1992**, *193*, 1181.
(9) Sotta, P.; Deloche, B. *Macromolecules* **1990**, *23*, 1999.
(10) Edwards, S. F.; McLeish, T. C. B. *J. Chem. Phys.* **1990**, *92*, 6855.
(11) Bastide, J.; Buzier, M.; Boué, F. In *Polymer Motion in Dense Polymer Systems*; Richter, D., Springer, T., Eds.; Springer: Berlin, 1988.
(12) Straube, E.; Urban, V.; Pyckhouthintzen, W.; Richter, D.; Glinka, C. J. *Phys. Rev. Lett.* **1995**, *74*, 4464.
(13) Read, D. J.; McLeish, T. C. B. *Phys. Rev. Lett.* **1997**, *79*, 87.
(14) Barea, J. L.; Muller, R.; Picot, C. In *Polymer Motion in Dense Polymer Systems*; Richter, D., Springer, T., Eds.; Springer: Berlin, 1988.
(15) Oeser, R.; Picot, C.; Herz, J. *Polymer Motion in Dense Polymer Systems*; Richter, D.; Springer, T., Eds.; Springer: Berlin, 1988.
(16) Ao, X.; Wen, X.; Meyer, R. B. *Physica A* **1991**, *176*, 63.
(17) Kamien, R. D.; Le Doussal, P.; Nelson, D. R. *Phys. Rev. A* **1992**, *45*, 8727.
(18) Kamien, R. D.; Grest, G. S. *Phys. Rev. E* **1997**, *55*, 1197.
(19) Boué, F.; Farnoux, B.; Bastide, J.; Lapp, A.; Herz, J.; Picot, C. *Europhys. Lett.* **1986**, *1*, 637.
(20) Sotta, P.; Higgs, P. G.; Depner, M.; Deloche, B. *Macromolecules* **1995**, *28*, 7208.
(21) Depner, M.; Deloche, B.; Sotta, P. *Macromolecules* **1994**, *27*, 5192.
(22) Baljon, A. R. C.; Grest, G. S.; Witten, T. A. *Macromolecules* **1995**, *28*, 1835.
(23) Haslam, A. J.; Jackson, G.; McLeish, T. C. B. *J. Chem. Phys.* **1999**, *111*, 416.
(24) Kuhn, W. *Kolloid-Z* **1934**, *68*, 2; Kuhn, W.; Grun, F. *Kolloid-Z* **1942**, *101*, 248.
(25) Šolc, K.; Stockmayer, W. H. *J. Chem. Phys.* **1971**, *54*, 2756.
(26) Šolc, K. *J. Chem. Phys.* **1971**, *55*, 335.
(27) Mazur, J.; Guttman, C.; McCrackin, F. *Macromolecules* **1973**, *6*, 872.
(28) Gobush, W.; Šolc, K.; Stockmayer, W. H. *J. Chem. Phys.* **1974**, *60*, 12.
(29) Kranbuel, E.; Verdier, P. H. *J. Chem. Phys.* **1977**, *67*, 361.
(30) Hansen, J. P.; McDonald, I. R. *Theory of Simple Liquids*, 2nd ed.; Academic Press: New York, 1986.
(31) Press, W. H.; Teukolsky, S. A.; Vetterling, W. T.; Flannery, B. P. *Numerical Recipes in Fortran, The Art of Scientific Computing*, 2nd ed.; Cambridge University Press: Cambridge, U.K., 1992.
(32) Abramovitz, M.; Stegun, A. S. *Handbook of Mathematical Functions*; Dover: London, 1964; p 360.

MA9802125